OPEN ACCESS
Journal of Innovative Optical Health Sciences
Vol. 14, No. 3 (2021) 2150013 (11 pages)

DOI: 10.1142/S1793545821500139

World Scientific
www.worldscientific.com

A novel indocyanine green-based fluorescent marker for guiding surgical tumor resection

Jiawei Ge[*,†,**], Justin D. Opfermann[*,‡], Hamed Saeidi[*,†], Katherine A. Huenerberg[§], Christopher D. Badger[¶], Jaepyeong Cha[‡], Martin J. Schnermann[‖], Arjun S. Joshi[¶] and Axel Krieger[*,†]

[*]*Department of Mechanical Engineering*
Johns Hopkins University
Baltimore, MD 21218, USA

[†]*Department of Mechanical Engineering*
University of Maryland
College Park, MD 20742, USA

[‡]*Sheikh Zayed Institute for Pediatric Surgical Innovation*
Children's National Hospital
Washington, DC 20010, USA

[§]*Department of Pathology*
George Washington University
Washington, DC 20052, USA

[¶]*Division of Otolaryngology - Head and Neck Surgery*
George Washington University
Washington, DC 20052, USA

[‖]*Chemical Biology Laboratory, Center for Cancer Research*
National Cancer Institute, National Institutes of Health
Frederick, MD 21702, USA
[**]*jge9@jhu.edu*

Received 15 March 2021
Accepted 16 March 2021
Published 23 April 2021

Surgical tumor resection is a common approach to cancer treatment. India Ink tattoos are widely used to aid tumor resection by localizing and mapping the tumor edge at the surface. However, India Ink tattoos are easily obscured during electrosurgical resection, and fade in intensity over time. In this work, a novel near-infrared (NIR) fluorescent marker is introduced as an alternative. The NIR marker was made by mixing indocyanine green (ICG), biocompatible cyanoacrylate, and acetone. The marking strategy was evaluated in a chronic *ex vivo* feasibility study using

[**]Corresponding author.

porcine tissues, followed by a chronic *in vivo* mouse study while compared with India Ink. In both studies, signal-to-noise (SNR) ratios and dimensions of the NIR markers and/or India Ink over the study period were calculated and reported. Electrocautery was performed on the last day of the mouse study after mice were euthanized, and SNR ratios and dimensions were quantified and compared. Biopsy was performed at all injection sites and slides were examined by a pathologist. The proposed NIR marker achieved (i) consistent visibility in the 26-day feasibility study and (ii) improved durability, visibility, and biocompatibility when compared to traditional India Ink over the six-week period in an *in vivo* mouse model. These effects persist after electrocautery whereas the India Ink markers were obscured. The use of a NIR fluorescent presurgical marking strategy has the potential for intraoperative tracking during long-term treatment protocols.

Keywords: Near-infrared fluorescent marker; surgical tumor resection; fluorescence-guided surgery; electrosurgery; India ink.

1. Introduction

Surgical tumor resection is a common cancer treatment, however some tumors may be initially unresectable due to large size or metastasis. For inoperable tumors, neoadjuvant therapies are used to induce tumor shrinkage and control metastasis so the tumor can be resected. This technique is used for many cancers including: pancreatic cancer, colorectal cancer with liver metastasis, bladder cancer, advanced melanoma, non-small cell lung cancer, and oropharyngeal cancer.[1–9] Before initiating neoadjuvant therapy, a patient is diagnosed *via* biopsy and staged with the aid of computed tomography, magnetic resonance images, or positron emitting tomography. It is common practice to localize and map the primary tumor edge at the surface by India Ink tattooing.[7,10–13] Tattooing is particularly useful when neoadjuvant treatment results in a dramatic decrease in the size of the primary tumor. When the tumor shrinks, the ink marker preserves location of the initial tumor bed which enables oncologically sound resection with adequate margins. Narrow margins are associated with recurrences, which may negatively impact survival. Likewise, an overly wide margin may impair post-surgical functioning.[14–16] Hence, maintaining a tumor-free resection margin after tissue distortion from neoadjuvant treatment effects is paramount to oncological outcomes.

Robotic-assisted surgery (RAS) is the standard of care for some surgical tumor resections.[17–20] RAS is often associated with minimally invasive surgery and incorporates surgical instrumentation previously unavailable with traditional approaches. Robotic manipulators for example, provide surgeons with high-resolution endoscopic visualization, and dexterous, tremor-free tools to achieve precise tele-operated tumor resection. Unfortunately, intraoperative tumor delineation with India Ink is prone to error during RAS because the ink markers are easily obscured by blood and charred tissue from electrocautery. Furthermore, India ink tattoos fade in intensity and size over the course of neoadjuvant therapy. While India Ink tattooing relies on direct surgeon visualization or the optics of traditional cameras, RAS can incorporate near-infrared (NIR) imaging systems capable of detecting high contrast NIR fluorescent markers in the surgical field. Our prior work demonstrated the feasibility of integrating a NIR image guided autonomous robotic system to guide surgical tasks.[21,22] Additionally, a NIR imaging system (Firefly, Intuitive Surgical, Sunnyvale, CA) is currently integrated with the da Vinci Surgical System (DVSS) (Intuitive Surgical, Sunnyvale, CA) for clinical use.

Advances in tumor imaging have improved the surgeon's ability to accurately delineate and resect cancerous tissues using RAS. One of the methods is fluorescence-guided surgery (FGS).[23] Fluorescent dyes conjugated to tumor-specific monoclonal antibodies are capable of selectively illuminating cancer cells to produce high contrast tumors. Bevacizumab-800CW is one such dye that has been used in phase I trials to identify rectal and esophageal cancer, and phase II trials to identify breast cancer. Two of the most researched agents, cetuximab-IRDye800CW and panitumumab-IRDye800CW, are under phase II trial studies identifying squamous cell carcinoma in the head and neck region.[24] However, these imaging agents are

not durable, and are usually dispensed to patients two to five days prior to surgery.[24] Additionally, the cancerous region highlighted by tumor specific dyes will shrink during neoadjuvant therapy. For long-term protocols with several cycles of neoadjuvant chemotherapy, decreases in tumor volume may be significant,[25] and these imaging agents fail to identify the original tumor beds which are typically removed with the remaining tumor.

In this paper, a novel tumor marking strategy is demonstrated to guide RAS tumor resections. Like the current clinical standard of care, we propose to preoperatively inject novel NIR fluorescent markers along the edge of the tumor bed. Unlike the current standard of care, the NIR signal emitted from the NIR markers can be observed intraoperatively via endoscopes regardless of blood and tissue charring. Furthermore, the stability of the NIR markers enables them to be embedded prior to neoadjuvant therapy. This approach allows the initial tumor bed to be identifiable during surgery. Ultimately, this work may lead to improved clinical outcomes due to better visible marking of the initial tumor bed during resection. Compared to India Ink, our NIR marker offers improved (i) visibility with high signal to noise ratios (SNRs), (ii) durability of at least six weeks, (iii) biocompatibility, and (iv) persistent visibility when electrocautery is used. We have previously demonstrated that the NIR fluorescent marker could be captured through blood and millimeter-thick tissue occlusion.[26,27] In this work, the proposed NIR marker's signal strength and durability was first evaluated in a chronic *ex vivo* feasibility study using porcine cadaver tissues. Next, we conducted a six-week *in vivo* mouse study to compare the fluorescent stability of the NIR marker to the standard India ink tattoo. Third, intraoperative visibility of each marker was quantified at the end of the survival period by measuring the SNR before and after electrocautery of the injection sites. Finally, histologic analysis of injection sites was also performed.

2. Materials and Methods

2.1. *Imaging system*

An imaging system to record NIR and color images (Fig. 1(a)) was mounted to an aluminum frame (80/20 Inc, Columbia City, IN) and placed in a box covered by blackout drape to achieve constant

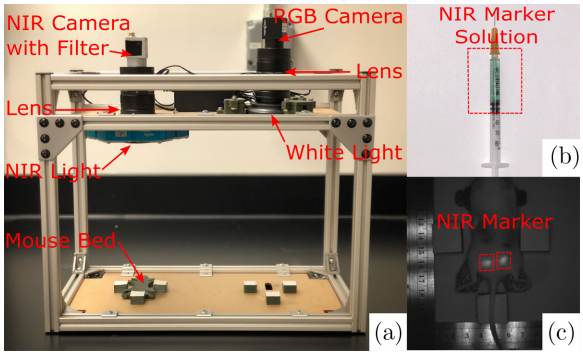

Fig. 1. (a) Imaging system with NIR and color cameras, (b) Color image of NIR marker solution in the syringe, and (c) NIR image of mouse #5 on the last study day showing two implanted NIR markers.

lighting conditions. The NIR imaging components consisted of (i) a NIR camera (Basler ace acA2040-90umNIR) (Basler AG, Ahrensburg, Germany), (ii) a band-pass filter (ET845/55m) (Chroma Technology, Bellows Falls, VT), (iii) a lens (Fujinon HF12.5SA-1) (Fujifilm, Tokyo, Japan), and (iv) a 760 nanometer NIR light-emitting diode (LED) (North Coast Technical Inc., Chesterland, OH). The NIR light source and filter were selected according to the peak excitation and emission wavelength of whole blood containing 0.05 mg/ml of sterile indocyanine green (ICG) (Akorn Inc., Lake Forest, IL), which were 805 nm and 835 nm, respectively. A 760 nm peak emission wavelength was chosen for the light source to account for the Gaussian spectral shapes of LEDs so that the light source provided adequate intensity for ICG excitation while avoiding light reflections at the observation wavelength. The light source was turned on one hour before imaging to allow the LED intensity to stabilize. The color imaging components were comprised of (i) a color charge-coupled camera (Point Grey FL2G-13S2C-C) (FLIR Systems, Wilsonville, OR), (ii) the same lens as used for NIR imaging, and (iii) a white light LED (AmScope LED-64-ZK) (United Scope LLC, Irvine, CA). A 3D printed platform was centered in the frame of each camera to ensure consistent placement of the mouse when imaging.

2.2. *Near-infrared fluorescent marker*

The NIR fluorescent marker was made by mixing 2 mg of clinical grade ICG (Akorn Inc., Lake Forest, IL), 0.5 ml acetone (Sigma-Aldrich, St. Louis, MO),

and 0.2 ml cyanoacrylate. Acetone was used as a solvent for the ICG, and is recognized to have low acute and chronic toxicity.[26] For consistent mixtures, the ICG and acetone solution was sonicated at 20% power for 45 s using a Q55 Sonicator (Qsonica, Newtown, CT). After sonication, cyanoacrylate was added to the mixture and loaded into a 1 ml syringe (Fig. 1(b)). The NIR solution remains liquid in the syringe until it is injected into target tissue. Once injected, the NIR solution polymerizes and the NIR fluorescence are triggered (Fig. 1(c)). In this work, we investigated the effect of two cyanoacrylates on NIR fluorescence. Notably, both cyanoacrylates polymerized when in contact with animal tissues, encapsulated ICG fluorescence, and did not migrate in the tissue once injected. However, both cyanoacrylates had different biochemical and physiologic characteristics. Permabond (McMaster-Carr, Elmhurst, IL) was used for the *ex vivo* feasibility study. Permabond is a short-chain ethyl 2-cyanoacrylate, which is bacteriostatic, fast-acting, affordable, but toxic.[28] LiquiBand Flow Control (Advanced Medical Solutions Ltd, Winsford, UK) was used for the chronic *in vivo* study. LiquiBand is a long-chain *n*-butyl cyanoacrylate that when compared to Permabond, polymerizes slower (< 30 s), degrades slower, and bonds stronger to native tissues.[28] Most importantly, LiquiBand is FDA approved with minimal toxicity.

2.3. *Animal model and study design*

The chronic *ex vivo* feasibility study was performed using three porcine cadaver tongues and two cheeks. Permabond was used as the cyanoacrylate in the NIR marker solution. Each injection was 0.03 ml, and considered to be one NIR marker. Using 26 gauge needles, four NIR markers were subcutaneously injected for each sample (tongue NIR marker $N = 12$, cheek NIR marker $N = 8$). NIR images of each sample were taken once per day for the first five days, and then the samples were frozen. On day 26, all samples were thawed, and a final image of each sample was taken.

The chronic *in vivo* comparison study was approved by the Institutional Animal Care and Use Committee (IACUC) at Children's National Hospital under protocol #30603. Five white A/J adult male mice were used (Jackson Laboratories, Bar Harbor, ME). LiquiBand was used as the cyanoacrylate in the NIR marker solution as described in Sec. 2.2. Each NIR marker consisted of 0.03 ml of the NIR solution. The NIR solution and India Ink were prepared using sterile technique. For each mouse, two NIR markers were subcutaneously injected using a 26 gauge needle in the bottom flank (NIR marker $N = 10$), and two India Ink markers were tattooed using 20 gauge needles on the top flank (ink marker $N = 10$). NIR and color images of all markers were recorded twice per week for six weeks to replicate a two-cycle period of chemotherapy.[8,9] Prior to imaging each day, the mice were anesthetized with isoflurane, placed in the prone position, and flanks shaved. Bodyweight measurements for each mouse were performed after each imaging session.

On day 43, mice fur was removed using a depilatory lotion (Nair) (Church & Dwight Co., Inc., Ewing, NJ). Depilation was performed to imitate many surgical tumor resection scenarios where there are no hair follicles covering tissues. NIR and color images were recorded, and the mice were euthanized. To mimic intraoperative blood and charred tissue interference observed during tumor resection, electrocautery was used to remove a small skin flap within the four markers on mouse flanks. After electrosurgery, the mice were imaged one final time. Upon completion of the study, each injection site was resected and fixed with 10% neutral buffered formalin for one week. The samples were embedded in paraffin, and 5-μm sections were stained with hematoxylin-eosin. Twenty slides were examined (ten NIR & ten ink markers) by a pathologist. The skeletal muscle in each tissue section was assessed for the presence of acute and chronic inflammation, necrosis, and other noteworthy histopathologic features.

To quantify the fluorescence efficiency of the NIR marker over electrocautery induced heat, an *ex vivo* study was performed. NIR markers ($N = 27$) were dispensed on the top surface of porcine cadaver tongue cuts ($N = 15$) to simulate tumor margins. Three drops of Permabond-based marker solution using a 20 gauge bevel needle were considered as one marker. After each NIR marker was dispensed, electrocautery was performed around each marker with 3 mm incision depth and various resection margin ($N \in \{1, 2, 3, 4\}$ mm). The resection margins are intentionally smaller than 5 mm so that temperatures near each marker would be higher than what is observed during clinical electrosurgery.[29–31] Peak temperature for each marker was recorded in

degrees Celsius using a digital multimeter DM6000AR (AstroAI, Placentia, CA). NIR images of each sample were recorded before and after the electrocautery procedure.

2.4. *Image quantification and statistical analysis*

Grayscale bmp (2048×2048 pixels) and color tiff (1280×960 pixels) format images were acquired for NIR and ink markers, respectively. Camera parameters were pretuned to minimize color saturation. Matlab (MathWorks, MA) scripts were customized to quantify marker SNRs and areas. Grayscale values were used directly as the NIR marker signal unit. Color images were converted to CMYK color mode and used K (black) channel as an ink marker signal unit. Thresholding based on the three-sigma control method was successfully used for pattern recognition,[32,33] and employed in this work for both NIR and color markers. Mean background intensity μ_b was computed in Eq. (1), where a number set I_b saved signal intensity values of all m pixels on clean mouse skins.

$$\mu_b = \left(\sum_{i=1}^{m} I_{b_i}\right) \Big/ m. \tag{1}$$

Standard deviation of background intensity σ_b was computed using the following equation:

$$\sigma_b = \sqrt{\left(\sum_{i=1}^{m} I_{b_i} - \mu_b)^2\right) \Big/ (m-1)}. \tag{2}$$

Pixels with signal intensity values greater than $\mu_b + 3\sigma_b$ were preserved as marker signals and saved in a number set I_m.

$$\{I_m | I_m > \mu_b + 3\sigma_b\}. \tag{3}$$

Filtering was performed by preserving the brightest 35% pixels to match visual intuition. Set I_m containing n pixels was ranked in descending order to yield the set I_{mr}, and updated using the following equation:

$$I_m = \bigcup_{i=1}^{n} \begin{cases} I_{m_i}, & I_{m_i} \geq I_{mr_{\text{integer}(0.35n)}} \\ \emptyset, & I_{m_i} < I_{mr_{\text{integer}(0.35n)}} \end{cases}. \tag{4}$$

Replacing set I_b with updated set I_m in Eq. (1) yielded mean marker intensity μ_m, and the marker SNR was defined as follows:

$$\text{SNR} = \mu_m / \mu_b. \tag{5}$$

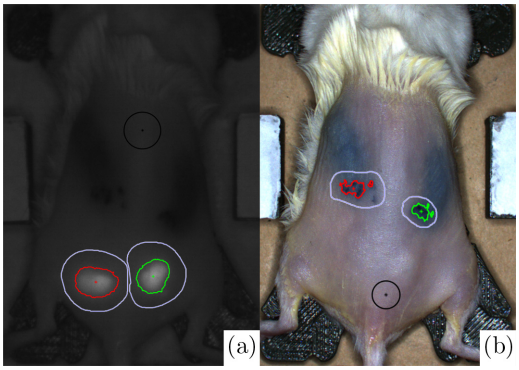

Fig. 2. (a) NIR and (b) color images of depilated mouse #5 on the last study day. Black circles and purple outlines are manually chosen for a clean background, and region of interest containing one marker, respectively. Red and green areas are marker areas yielded from the customized Matlab image quantification.

The number of pixels in the updated set I_m equaled to marker area in pixels. Pixel-to-millimeter scale was extracted using a ruler in the field of view on the same height as mouse flanks (Fig. 1(c)), to calculate marker area in mm^2. Figure 2 shows the inputs and results of the image quantification process on a sample image set. The fluorescence efficiency η in reaction to temperature increase due to electrocautery was defined in the following equation:

$$\eta = 100\% * \text{SNR}_{\text{post-cautery}} / \text{SNR}_{\text{pre-cautery}}. \tag{6}$$

After SNR and area calculations, an analysis of variance (ANOVA) test was used to analyze differences in results among all experimental days for *ex vivo* and *in vivo* studies. The student t-test was used to compare NIR and ink marker SNRs on the last study day for the *in vivo* study. Moreover, marker SNR calculations were performed two more times for mouse images acquired on the last study day, once for the images after fur depilation, and once after electrocautery. For the electrocauterized mouse image calculations, an area of electrocauterized tissue was used for the background. The student t-test was performed to analyze electrocautery's influence on NIR and ink markers. A significance level of 0.05 was used for all ANOVA and student t-tests.

3. Results

3.1. *Chronic ex-vivo feasibility study*

NIR markers were injected into porcine cadaver tongues and cheeks and the resulting SNR for each

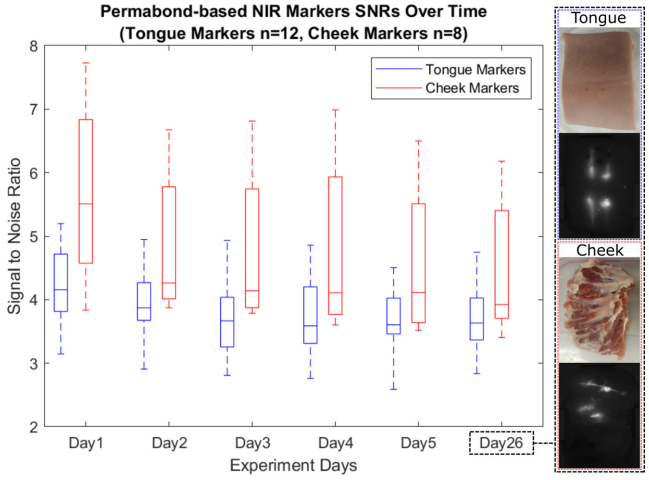

Fig. 3. Box plot of the Permabond-based marker signal to noise ratios over time in the chronic *ex vivo* study. Color and NIR images of a tongue and a cheek sample at day 26 are shown as well.

marker was quantified over a period of 26 days as illustrated in Fig. 3. From day 1 to day 26, porcine tongue and cheek NIR marker SNRs decreased from 4.23 ± 0.63 to 3.70 ± 0.51, and from 5.68 ± 1.46 to 4.46 ± 1.07, respectively. Both decreases in NIR marker signal contrast were not found to be statistically significant in ANOVA tests ($P = 0.111$ and $P = 0.440$, respectively).

3.2. *Chronic in-vivo mouse study – marker visibility and dilation over time*

To determine the fluorescent and positional stability of the NIR markers on shaved mice, SNRs and surface areas for each marker were calculated for a period of 43 days as illustrated in Figs. 4(a) and 4(b). An initial washout period from day 1 to day 5 was observed in Fig. 4(a); SNR for NIR and India ink markers decreased from 2.39 ± 0.60 to 1.84 ± 0.43 and from 2.33 ± 0.28 to 1.83 ± 0.12, respectively. The initial washout of NIR markers was expected because the ICG solution can bind to plasma proteins that are excreted instead of encapsulating in the cyanoacrylate.[34,35] Similarly, India ink markers that were not tattooed deep enough to stain the epidermis were captured on day 1 but faded by day 5, leading to washout of the India ink.

From day 5 to day 43, NIR and India ink marker signals further dropped to 1.73 ± 0.21 and 1.50 ± 0.06, respectively. Notably, the average decrease in NIR marker signal from day 5 to day 43 was not found to be statistically significant ($P = 0.996$). In contrast, India Ink demonstrated a significant decrease in signal from day 5 to day 43 using a one-way ANOVA with post hoc Tukey test ($P < 0.001$). When NIR and India Ink SNR on day 43 were directly compared with a student t-test, NIR SNR was significantly greater ($P = 0.003$).

Figure 4(b) presents marker surface areas for shaved mice over the entire study period. Like the analysis of SNRs, both NIR and ink marker surface areas decreased during the first five days of the study from 61.63 ± 13.92 to $26.21 \pm 7.02\,\text{mm}^2$ and from 28.86 ± 14.70 to $1.88 \pm 1.09\,\text{mm}^2$, respectively. Nevertheless, from day 5 to day 43, the average decrease in NIR and ink marker areas were not statistically significant ($P = 0.996$ and $P = 0.244$, respectively). Representative data from a mouse in shaved condition is reported in the first three columns of Fig. 4(d).

3.3. *Marker visibility changes caused by electrocautery*

Ink and NIR marker SNRs for depilated (Naired) and electrocauterized mice on day 43 are presented in Fig. 4(c) to demonstrate SNR changes caused by electrocautery. Representative data from a mouse in depilated and electrocauterized conditions are shown in the last two columns of Fig. 4(d). After cauterization, ink marker SNRs dropped from 1.36 ± 0.09 to 1.09 ± 0.06 ($P < 0.001$), while NIR marker SNRs increased from 2.04 ± 0.29 to 2.17 ± 0.34 ($P = 0.176$). Although the increase in SNR for NIR markers was not significant, the trend towards increasing SNR suggests that the visibility of NIR markers is not diminished with electrocauterization. NIR marker SNRs were significantly higher compared to ink marker SNRs on day 43 after electrocautery ($P < 0.001$).

Permabond-based NIR marker fluorescence efficiency over electrocautery induced heat is reported in Fig. 4(e). The number of markers reaching a temperature of {18, 19, 20, 21, 22, 23, 24, 25, 28, 29, 30, 32, 35, 36, 37, 46, 48, 52}°C equaled to {3, 2, 1, 1, 1, 2, 1, 1, 3, 1, 2, 1, 1, 2, 1, 2, 1, 1}, respectively. An average fluorescence efficiency was presented if more than one marker shared the same

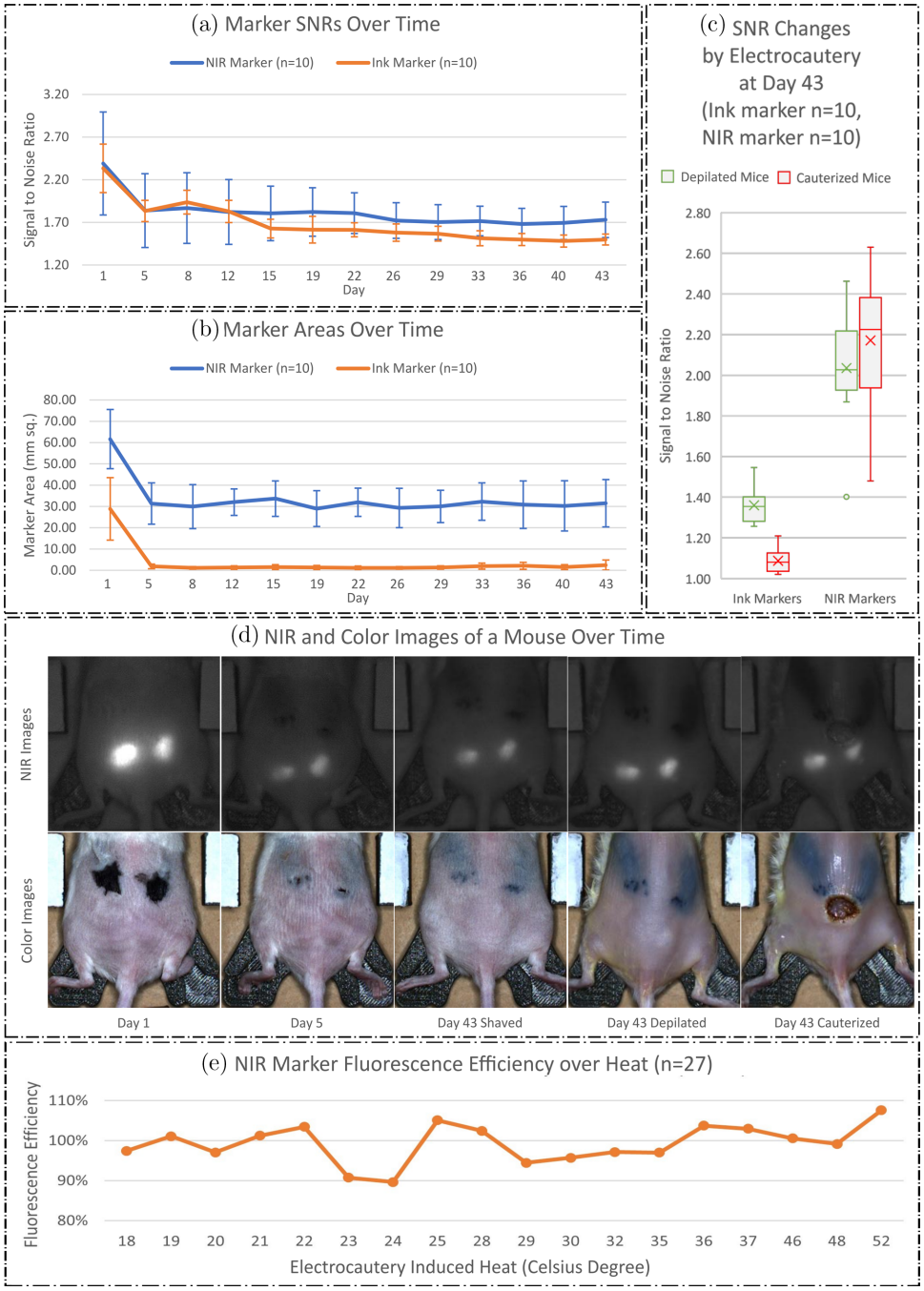

Fig. 4. (a) LiquiBand-based NIR and ink marker signal to noise ratios and (b) areas for shaved mice over the whole study period. (c) Box plots of ink and LiquiBand-based NIR marker signal to noise ratios on the day 43 for depilated and electrocauterized mice. (d) NIR and color images of mouse #5 on the day 1, 5, and 43 (shaved, depilated, and cauterized) are shown. (e) Graph of fluorescence efficiency of Permabond-based NIR marker over electrocautery induced heat.

temperature. The mean fluorescence efficiency over the full temperature range was 0.992 ± 0.054 ($N = 27$). No fluorescence efficiency decrease was observed at higher temperatures. The fluorescence efficiency of the proposed NIR marker was persistent to electrocautery induced heat up to 52°C.

3.4. *Chronic in-vivo mouse study – histology and weight*

Figure 5 illustrates representative histology of tissue at NIR (Fig. 5(a)) and India ink (Fig. 5(d)) injection sites. The NIR marker demonstrated a foreign body giant cell reaction at all 10 implantation sites.

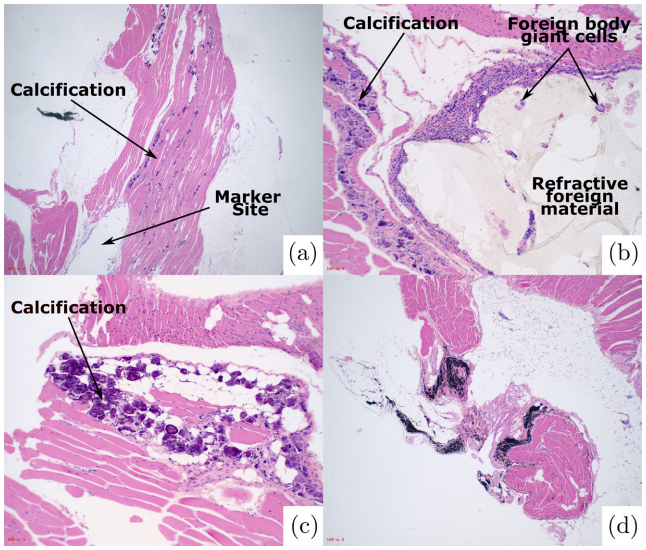

Fig. 5. (a)–(c) Histological appearance of NIR marker site. (a) Marker site is identified adjacent to linear calcifications within skeletal muscle. (b) Marker site is associated with a foreign body giant cell reaction with refractive foreign material. (c) Calcifications within skeletal muscle (10× magnification). (d) Histologic appearance of India Ink site.

Within this foreign body reaction, a refractive, nonpolarizable material was identified. India Ink was identified histologically in nine (of ten) injection sites. The presence of India Ink was associated with pigment laden macrophages.

In all 10 NIR marker samples, the foreign body giant cell reaction seen was associated with a calcific response within the skeletal muscle. These calcifications were distributed linearly and were not associated with a significant inflammatory response. In one India Ink case, a single calcification was identified within the skeletal muscle.

All slides were scanned at low power for the presence of acute inflammation and necrosis. No inflammation outside of the foreign body reaction and histiocytic inflammation was noted. No necrosis was identified. Ten high powered fields (HPF) (40× magnification) were then examined to assess for neutrophils. For the NIR marker cases, this assessment began one 20× field away from the site of the foreign body giant cell reaction. For all 20 slides reviewed (10 NIR & 10 ink markers), no neutrophils were identified (0/10 HPF).

The average weight of five mice dropped from 23.64 ± 1.39 to 19.10 ± 1.87 g from day 1 to day 5, and gradually increased to 22.16 ± 1.35 g from day 5 to day 43. The average weight on day 43 was significantly heavier than on day 5 ($P = 0.009$) but was not statistically different than weight on day 1 ($P = 0.063$). Initial weight loss in mice was expected since subcutaneous injection of normal saline can result in acute loss of bodyweight.[36]

4. Discussions

We proposed a novel technique for marking tumors using biocompatible NIR dyes and cyanoacrylates. This novel marker offers several advantages over the current clinical standard, India Ink tattooing. First, while electrocautery obfuscates ink markers, the NIR marker is robustly identifiable after electrocautery, and even demonstrates a trend towards increased SNRs in this setting. Second, the NIR marker remains clearly visible six weeks after placement without a significant decrease in SNR. As further research is done on the utility of neoadjuvant treatment protocols,[1–9] the need for a robust fiduciary of tumor margin is essential for the assessment of treatment response. The SNR and area results in this *in vivo* study demonstrate that the luminance and dimension of this NIR marker is durable over six weeks, which mimics two chemotherapy cycles.[8,9] Third, the NIR markers were more easily distinguished when directly compared to India Ink tattoos after six weeks in an *in vivo* model. Finally, the NIR marker was biocompatible in a mouse model without evidence of acute inflammation and necrosis during the study period. As a result, the NIR marker fluorescence could be easily and robustly tracked across a wide range of surgical conditions and time points.

While the NIR marker used in this study requires the use of a NIR camera, filter, and NIR LED, these components are ideal for incorporation and compatibility with existing RAS equipment. Surgeons acquire information like tissue textures and anatomic boundaries may be acquired from color cameras, while the NIR markers are synchronized and overlaid onto the color video stream in real-time. This image fusion is feasible and has been demonstrated in our prior works.[21,22] Alternatively, the capability of switching between color and NIR visual feedbacks in a robotic system is beneficial. As aforementioned, this technique is clinically available in the DVSS, where ICG fluorescence is visible with the Firefly system.

Admittedly, there exist limitations in this study. First, the study lacks a mucosal *in-vivo* analog. For the sake of animal accessibility, mice are used in this

study, and only flanks have the dimension for multiple marker implantation. Second, the study lacks a control group of mice with normal saline injections. The control group can help explain whether the observed weight loss on day 5 is triggered by mouse behavioral and stress reactions to subcutaneous injections, or by implanted markers. Third, the white light LED used in the study has a poor ability to accurately reproduce the colors of the object it illuminates. The color rendering index (CRI) of the white light LED is measured using the C-800 SpectroMaster Color Meter (Sekonic, Tokyo, Japan) in the normal measuring range setting. The average CRI equals 77.2, and the strong red color CRI (R9) equals −16.6. The white light LED is poor in average CRI, and has limited rendering ability of red color. The color rendering quality is not ideal but suitable for a validation study using *ex vivo* and *in vivo* animal models. A better artificial white light LED in terms of CRI will be used in our future work towards human trials in an operating room environment. Fourth, the marking strategy is designed for RAS, but no RAS experimental setup is presented in the study. We are planning to integrate the new NIR marking strategy in the DVSS and Firefly imaging system to evaluate if the demonstrated imaging advantages of the NIR markers over India Ink result in more precise tumor resections and margin controls for RAS. Tumors will be grown on mouse flanks, and tumor margins will be marked using India Ink and our NIR marker. Manual and autonomous tumor resection will be performed by surgeons and our robotic system,[21,22] respectively, relying on different marking methods. The surgical outcomes will be evaluated and compared.

The proposed manual NIR marking technique is not without limitations. Like India Ink, these markers are placed where they are easily visualized on a tissue surface. They do not provide the surgeon with any information regarding the depth of tumor invasion. However, this may be solved as targeting imaging agents, such as Bevacizumab-800CW, cetuximab-IRDye800CW and panitumumab-IRDye800CW[24] are further developed. These agents had similar NIR emission peak wavelengths, and could be captured by the optics system used in this study. The combination of our NIR marker and tumor-targeting imaging agents would allow for the comparison of the original tumor surface edges and the shrunken 3D tumor edges in response to various treatment protocols. This may facilitate and expedite treatment decisions in the future.

5. Conclusions

This study demonstrated the improved visibility, durability, and biocompatibility of an ICG-based NIR marker in an *in vivo* mouse model over a six-week period when compared with traditional India Ink tattooing methods. The advantages of a NIR marker persisted even after electrocautery of tissues. The NIR marker was robustly traceable and showed a trend towards increased SNR under the blood and charred tissue obfuscation. Our developed NIR marker potentially presents an improved alternative over India Ink as it outperformed India Ink in marking contrast and robustness against the noise caused by electrocautery.

Conflict of Interest

There is no conflict of interest to disclose.

Acknowledgments

This work is supported by the National Institutes of Health under award numbers 1R01EB020610 and R21EB024707, and supported by the Intramural Research Program of the National Institutes of Health, National Cancer Institute, Center for Cancer Research. The content is solely the responsibility of the authors and does not necessarily represent the official views of the National Institutes of Health.

References

1. C. Yoo, S. H. Shin, K. Kim *et al.*, "Clinical outcomes of conversion surgery after neoadjuvant chemotherapy in patients with borderline resectable and locally advanced unresectable pancreatic cancer: A single-center, retrospective analysis," *Cancers* **11**(3), 278 (2019). doi: 10.3390/cancers11030278.
2. W. L. Shaib, A. Ip, K. Cardona *et al.*, "Contemporary management of borderline resectable and locally advanced unresectable pancreatic cancer," *Oncologist* **21**(2), 178–187 (2016). doi: 10.1634/theoncologist.2015-0316.
3. M. Basso, V. Dadduzio, F. Ardito *et al.*, "Conversion chemotherapy for technically unresectable colorectal liver metastases," *Medicine*

(Baltimore) **95**(20), e3722 (2016). doi: 10.1097/MD.0000000000003722.

4. M. Abufaraj, K. Gust, M. Moschini *et al.*, "Management of muscle invasive, locally advanced and metastatic urothelial carcinoma of the bladder: a literature review with emphasis on the role of surgery," *Transl. Androl. Urol.* **5**(5), 735–744 (2016). doi: 10.21037/tau.2016.08.23.
5. J. Sun, D. A. Kirichenko, J. S. Zager, Z. Eroglu, "The emergence of neoadjuvant therapy in advanced melanoma," *Melanoma Manag.* **6**(3), MMT27 (2019). doi: 10.2217/mmt-2019-0007.
6. D. Uprety, S. J. Mandrekar, D. Wigle, A. C. Roden, A. A. Adjei, "Neoadjuvant immunotherapy for NSCLC: current concepts and future approaches," *J. Thorac. Oncol.* **15**(8), 1281–1297 (2020). doi: 10.1016/j.jtho.2020.05.020.
7. N. Sadeghi, N.-W. Li, M. R. Taheri, S. Easley, R. S. Siegel, "Neoadjuvant chemotherapy and transoral surgery as a definitive treatment for oropharyngeal cancer: A feasible novel approach," *Head Neck* **38** (12), 1837–1846 (2016). doi: 10.1002/hed.24526.
8. N. Sadeghi, M. A. Mascarella, S. Khalife *et al.*, "Neoadjuvant chemotherapy followed by surgery for HPV-associated locoregionally advanced oropharynx cancer," *Head Neck* **42**(8), 2145–2154 (2020). doi: 10.1002/hed.26147.
9. N. Sadeghi, S. Khalife, M. A. Mascarella *et al.*, "Pathologic response to neoadjuvant chemotherapy in HPV-associated oropharynx cancer," *Head Neck* **42**(3), 417–425 (2020). doi: 10.1002/hed.26022.
10. A. Patil, R. Anand, P. Mahajan, "Comparative study of acrylic color and India ink for their use as a surgical margin inks in oral squamous cell carcinoma," *World J. Dent.* **6**(1), 26–30 (2015). doi: 10.5005/jp-journals-10015-1308.
11. M. Yang, D. Pepe, C. M. Schlachta, N. A. Alkhamesi, "Endoscopic tattoo: the importance and need for standardised guidelines and protocol," *J. R. Soc. Med.* **110**(7), 287–291 (2017). doi: 10.1177/0141076817712244.
12. B. K. Kim, M. H. Song, H. J. Yang, D. S. Kim, N. K. Lee, Y. S. Jeon, "Use of cystoscopic tattooing in laparoscopic partial cystectomy," *Korean J. Urol.* **53**(6), 401–404 (2012). doi: 10.4111/kju.2012.53.6.401.
13. M. R. Hwang, D. K. Sohn, J. W. Park *et al.*, "Small-dose India ink tattooing for preoperative localization of colorectal tumor," *J. Laparoendosc. Adv. Surg. Tech. A*, **20**(9), 731–734 (2010). doi: 10.1089/lap.2010.0284.
14. R. Haque, R. Contreras, M. P. McNicoll, E. C. Eckberg, D. B. Petitti, "Surgical margins and survival after head and neck cancer surgery," *BMC Ear Nose Throat Disord.* **6**, 2 (2006). doi: 10.1186/1472-6815-6-2.
15. H. W. Herr, "Extent of surgery and pathology evaluation has an impact on bladder cancer outcomes after radical cystectomy," *Urology* **61**(1), 105–108 (2003). doi: 10.1016/S0090-4295(02)02116-7.
16. W. S. Tummers, J. V. Groen, B. G. Sibinga Mulder *et al.*, "Impact of resection margin status on recurrence and survival in pancreatic cancer surgery," *Br. J. Surg.* **106**(8), 1055–1065 (2019). doi: 10.1002/bjs.11115.
17. U. Boggi, N. Napoli, F. Costa *et al.*, "Robotic-assisted pancreatic resections," *World J. Surg.* **40**(10), 2497–2506 (2016). doi: 10.1007/s00268-016-3565-3.
18. G. Cheung, A. Sahai, M. Billia, P. Dasgupta, M. S. Khan, "Recent advances in the diagnosis and treatment of bladder cancer," *BMC Med.* **11**(1), 13 (2013). doi: 10.1186/1741-7015-11-13.
19. R. M. Jiménez Rodríguez, J. M. Díaz Pavón, F. de La Portilla de Juan, E. Prendes Sillero, J. M. Hisnard Cadet Dussort, J. Padillo, "Prospective randomised study: robotic-assisted versus conventional laparoscopic surgery in colorectal cancer resection," *Cir. Esp. Engl. Ed.* **89**(7), 432–438 (2011). doi: 10.1016/j.cireng.2011.01.001.
20. G. S. Weinstein, B. W. O'Malley, J. S. Magnuson *et al.*, "Transoral robotic surgery: a multicenter study to assess feasibility, safety, and surgical margins," *Laryngoscope* **122**(8), 1701–1707 (2012). doi: 10.1002/lary.23294.
21. H. Saeidi, J. Ge, M. Kam *et al.*, "Supervised autonomous electrosurgery via biocompatible near-infrared tissue tracking techniques," *IEEE Trans. Med. Robot Bionics.* **1**(4), 228–236 (2019). doi: 10.1109/TMRB.2019.2949870.
22. J. Ge, H. Saeidi, J. D. Opfermann, A. S. Joshi, A. Krieger, Landmark-guided deformable image registration for supervised autonomous robotic tumor resection, *Medical Image Computing and Computer Assisted Intervention – MICCAI 2019*, D. Shen, T. Liu, T. M. Peters *et al.*, Eds., pp. 320–328, Springer International Publishing (2019).
23. T. Nagaya, Y. A. Nakamura, P. L. Choyke, H. Kobayashi, "Fluorescence-guided surgery," *Front. Oncol.* **7**, 314 (2017). doi: 10.3389/fonc.2017.00314.
24. ClinicalTrials.gov (NCT02129933, NCT01972373, NCT02583568, NCT03134846, NCT03405142). Accessed June 14, 2020. https://clinicaltrials.gov/.
25. T. A. Dalsaso, V. J. Lowe, F. R. Dunphy, D. S. Martin, J. H. Boyd, B. C. Stack, "FDG-PET and CT in evaluation of chemotherapy in advanced head and neck cancer," *Clin. Positron Imaging Off J.*

Inst. Clin. PET **3**(1), 1–5 (2000). doi: 10.1016/s1095-0397(99)00074-6.

26. R. S. Decker, A. Shademan, J. D. Opfermann, S. Leonard, P. C. Kim, A. Krieger, "Biocompatible near-infrared three-dimensional tracking system," *IEEE Trans. Biomed. Eng.* **64**(3), 549–556 (2017).
27. A. Shademan, R. S. Decker, J. D. Opfermann, S. Leonard, A. Krieger, P. C. W. Kim, "Supervised autonomous robotic soft tissue surgery," *Sci. Transl. Med.* **8**(337), 337ra64 (2016). doi: 10.1126/scitranslmed.aad9398.
28. S. N. Ayyıldız, A. Ayyıldız, "Cyanoacrylic tissue glues: Biochemical properties and their usage in urology," *Turk. J. Urol.* **43**(1), 14–24 (2017). doi: 10.5152/tud.2017.09465.
29. A. F. Nahhas, C. A. Scarbrough, S. Trotter, "A review of the global guidelines on surgical margins for nonmelanoma skin cancers," *J. Clin. Aesthetic Dermatol.* **10**(4), 37–46 (2017).
30. S. G. Brouwer de Koning, M.-J. T. F. D. Vrancken Peeters, K. Jóźwiak, P. A. Bhairosing, T. J. M. Ruers, "Tumor resection margin definitions in breast-conserving surgery: systematic review and meta-analysis of the current literature," *Clin. Breast Cancer* **18**(4), e595–e600 (2018). doi: 10.1016/j.clbc.2018.04.004.
31. G. Vallancien, H. Abou el fettouh, X. Cathelineau, H. Baumert, G. Fromont, B. Guillonneau, "Cystectomy with prostate sparing for bladder cancer in 100 patients: 10-year experience," *J. Urol.* **168**(6), 2413–2417 (2002). doi: 10.1016/S0022-5347(05)64157-2.
32. M. S. Ahmed, B. Indira, Detection of exudates from RGB fundus images using 3σ control method, *2017 Int. Conf. Wirel Commun. Signal Process Netw. WiSPNET*. Published online 2017. doi: 10.1109/wispnet.2017.8299864.
33. A. Danti, Suresha, "Segmentation and classification of raw arecanuts based on three sigma control limits," *Proc. Technol.* **4**, 215–219 (2012). doi: 10.1016/j.protcy.2012.05.032.
34. S. Yoneya, T. Saito, Y. Komatsu, I. Koyama, K. Takahashi, J. Duvoll-Young, "Binding properties of indocyanine green in human blood," *Invest. Ophthalmol. Vis. Sci.* **39**(7), 1286–1290 (1998).
35. J. T. Alander, I. Kaartinen, A. Laakso *et al.*, "A review of indocyanine green fluorescent imaging in surgery," *Int. J. Biomed. Imaging* **2012**, 940585 (2012). doi:https://doi.org/10.1155/2012/940585.
36. P. Jirkof, A. Tourvieille, P. Cinelli, M. Arras, "Buprenorphine for pain relief in mice: Repeated injections vs sustained-release depot formulation," *Lab Anim.* **49**(3), 177–187 (2015). doi: 10.1177/0023677214562849.